Available online at www.sciencedirect.com

ScienceDirect

IFAC Papers Online CONFERENCE PAPER ARCHIVE

IFAC-PapersOnLine 49-26 (2016) 020–025

Bringing the parts together: Steps towards an in-silico protocell

Eugenia Schneider * **Jakob Schweizer** ** **Michael Mangold** ***

* *Max-Planck-Institute for Dynamics of Complex Technical Systems, 39106 Magdeburg, Germany (e-mail: eschneider@mpi-magdeburg.mpg.de).*

** *Max-Planck-Institute for Dynamics of Complex Technical Systems, 39106 Magdeburg, Germany*

*** *Max-Planck-Institute for Dynamics of Complex Technical Systems, 39106 Magdeburg, Germany (e-mail: mangold@mpi-magdeburg.mpg.de)*

Abstract: This article focuses on a system theoretic approach to synthetic biology, and in particular on the construction of a protocell model. The questions addressed here are: Which parts of functional modules are required to describe a protocell and which design methods are needed for self-replicating systems. We describe a model for an in-silico protocell that combines experimentally validated biological subsystems with theoretical studies.

Keywords: systems engineering, system analysis, synchronization, synthetic biology, bottom-up approach, artificial cell

1. INTRODUCTION

Synthetic Biology aims at creating new life forms with beneficial properties for chemical, pharmaceutical, or medical applications (Keasling, 2008; Trosset and Carbonell, 2015) but also plays a major role in the fundamental research. The top-down approach of Synthetic Biology, which equips existing organisms with additional capabilities, has recently proven to be feasible for solving technical problems in fuel production and drug production (Keasling, 2012). The complementary bottom-up approach, which tries to build life-like entities from molecular building blocks, is still in its infancy, but in the future may have the potential to provide simple, safe, and well predictable artificial organisms tailored to certain applications (Schwille, 2011).

Currently, the bottom-up approach is mainly driven by biophysical groups, who concentrate on mimicking certain cellular functions like membrane growth, cell division, or cell motility in experiments. Assembling these functions to an aggregate unit is the logical next step, but experimentally very challenging. The question is if one can construct artificial cell-like entities from certain functional devices in a similar way, as one can construct a chemical plant from process units. At this point, there is an obvious link to chemical engineering, systems engineering, and control engineering (Rollié et al., 2012). Engineering sciences are used to combine parts to complex systems with certain well-defined desired properties of the resulting aggregate system, and, in this sense, are mainly target-oriented. This could be a nice complement to the insight-driven approach of natural sciences that strives for understanding a certain part aspect in full detail.

This work uses a simple example of an artificial biological system to discuss possible engineering contributions to bottom-up Synthetic Biology. The idea is to define a certain desired functionality of the artificial system, to select building blocks that may fulfill the desired tasks and to assemble the models of the building blocks to a simple in-silico protocell. There are experimental results and mathematical models for the separate building blocks in literature, but the aggregate system has not been implemented in experiments yet. The aim of the theoretical study is to see if the selected building blocks are able to work in an ensemble, or if additional functionalities like control mechanisms are needed.

It should be noted that detailed whole-cell models built up from submodels exist in literature for real-life biological organisms, e.g. Karr et al. (2012). However, due to the complexity of biological organisms, these models tend to be very large and offer only a limited accessibility to theoretical analysis. The hope is that artificial biological systems are much simpler in their behavior, and that hence their system dynamics can be described and predicted more easily by smaller sets of mathematical equations.

2. STRUCTURED MODEL OF AN ARTIFICIAL CELL-LIKE ENTITY

The exemplary design task considered in the following is the construction of an entity that has the ability to grow, to determine the time point when its size has doubled compared to the original value, and finally to divide into two daughter cells. For this purpose, at least three different functional modules are needed. The first one is a container that forms the system boundary and grows, while its building blocks are generated inside the system. The second functional module is a length sensor that determines the position where the cell should divide. The third module is a divisome that performs the cell

10.1016/j.ifacol.2016.12.097

division by placing a contractile ring in the middle of the cell. In reality, at least one additional functional module would be needed for ATP regeneration as an energy supply. This is neglected here. For simplicity, it is assumed that the ATP level is always high enough to drive the required reactions. The models of the single modules presented in the following are largely taken from literature and adapted to our needs. The combination of the three parts to an artificial cell model is, to our knowledge, something new.

2.1 Expanding container

Mavelli et al. (2014) suggest a simple model for the growth of a vesicle or expanding container shown in Fig. 1.

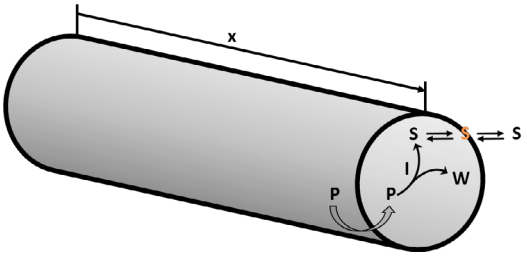

Fig. 1. Functional module-tube shaped membrane. P is a precursor, I is an enzyme, S is the surfactant and W is the waste (Mavelli et al., 2014). x denotes the length of the cylindric compartment.

A precursor P is metabolized by an enzyme I into a surfactant S and a waste W. The surfactant S is included along the entire membrane and increases its surface by a certain amount. While Mavelli et al. (2014) formulate a well-mixed model, we extend the approach to an one-dimensional spatially distributed system, assuming that our artificial cell is tube shaped with a variable length x, but a constant radius R. This assumption is mainly made to simplify the numerical computations, but is not unrealistic for some rod-shaped bacteria. A mass balances of the species P, S, and I lead to the balance equations (1)-(3):

$$\frac{\partial(R^2P)}{\partial t} + \frac{\partial(R^2P\dot{x})}{\partial x} = -\frac{\partial(R^2 j_P)}{\partial x} - R^2 r_S + 2R\wp(P_{ex} - P) \quad (1)$$

$$\frac{\partial(R^2S)}{\partial t} + \frac{\partial(R^2S\dot{x})}{\partial x} = -\frac{\partial(R^2 j_S)}{\partial x} + R^2 r_S - R^2 r_{up} \quad (2)$$

$$\frac{\partial(R^2I)}{\partial t} + \frac{\partial(R^2I\dot{x})}{\partial x} = -\frac{\partial(R^2 j_I)}{\partial x} \quad (3)$$

The concentration change of the precursor P depends on the precursor mass diffusion flow j_P, the surfactant formation rate r_S, and the membrane permeability of the precursor $\wp$. R is the radius of the cylinder and P_{ext} is the extracellular precursor concentration. The surfactant formation rate r_S is calculated as follows:

$$r_S = kIP, \quad (4)$$

where k is the rate constant for the surfactant formation. The term $\dot{x}$ in the equations (1)-(3) denotes the local length change due to growth of the cell; it has a diluting effect on the concentrations. Similarly, the surfactant concentration S in the bulk of the cell depends on diffusive transport j_S, the formation rate r_S, and an uptake rate r_{up}, which describes the transfer of surfactants to the membrane; r_{up} depends on an equilibrium surfactant concentration S_{eq} and is given as:

$$r_{up} = k_{up}(S - S_{eq}); \quad (5)$$

k_{up} is the rate constant for the surfactant uptake into the membrane. The concentration of the enzyme I changes locally due to diffusion, but in a growing cell also globally due to dilution caused by increasing cell volume. For unlimited growth, the dilution effect would have to be compensated by synthesizing I inside the cell or by providing additional I from outside. This is not done here. Instead, the initial value of I in the simulations is chosen sufficiently high to guarantee surfactant formation until the cell size has at least doubled.

It is assumed that the surfactant S built into the membrane contributes to area of the membrane with a specific surface α_s. Calculating the surface of the cylinder leads to the relation:

$$2\frac{\partial R}{\partial t} + 2\frac{\partial(R\dot{x})}{\partial x} = \frac{\alpha_S}{2} R^2 r_{up} \quad (6)$$

which is used to determine the local growth rate $\dot{x}$ for a given radius R.

2.2 Length sensor/positioner

The Min protein system that is an important mechanism in the cell division of *E.coli* is known to exhibit spatial concentration patterns on membrane surfaces. The pattern formation capability in combination with the property of $MinC$ to prevent proteins from attaching to the membrane is supposed to control the cell division of *E.Coli*: A contractile protein ring is placed in the middle of the cell membrane, where the time averaged concentration of Min proteins on the membrane has been shown to be lowest (Huang et al., 2003; Loose et al., 2008; Schweizer et al., 2012). Fig.2 shows a qualitative model of the interaction between the Min proteins and the membrane surface. $MinD$ proteins labeled by the energy rich ATP molecule are able to attach to the membrane. This attachment occurs primarily on membrane regions where already other $MinD$ proteins are attached. The membrane associated $MinD$ protein recruits the $MinE$ protein and a complex formation results. The $MinE$ protein in the complex causes the hydrolysis of the bound ATP molecule, the detachment of the $MinD : MinE$ complex from the membrane and the detachment of the $MinE$ protein from the $MinD$ protein. Finally, the $MinD$ protein is situated in the cytosol binding the less energy rich molecule ADP and the cycle can start again.

The intracellular concentration changes of the Min proteins are calculated by the balance equations (7)-(11) and the reaction kinetics characterized by the equations (12)-(15). The concentration changes of the intracellular Min proteins depend on the mass diffusion flows $j_{D_{ADP}}$, $j_{D_{ATP}}$, j_E and $j_{D_{ADP}}$ as well as the reaction kinetics r_1, r_2, r_3 and r_4 describing the formation of cytosolic $MinD_{ADP}$, membrane bound $MinD_{ATP} : E$, membrane bound $MinD_{ATP}$ and cytosolic $MinD_{ATP}$, respectively.

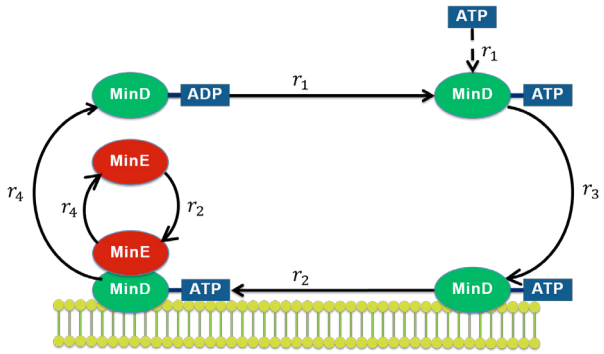

Fig. 2. Functional module-length sensor/positioner is represented by the energy driven $MinE$-$MinD$-protein cycle (Huang et al., 2003). $r1$: ADP that bounds to the intracellular $MinD$ protein is replaced by the more high energy molecule ATP. $r3$: $MinD_{ATP}$ bounds to the membrane primarily at locations where already other $MinD_{ATP}$ proteins are bound. $r2$: The intracellular protein $MinE$ bounds to a membrane associated $MinD_{ATP}$ and trigger the ATP hydrolysis into ADP and a phosphate, the detachment of the $MinE$ from $MinD$ and the detachment of $MinD$ from the membrane ($r4$).

The membrane bound components are denoted by $*$ in the balance equations:

$$\frac{\partial(R^2 D_{ADP})}{\partial t} + \frac{\partial(R^2 D_{ADP}\dot{x})}{\partial x} = -\frac{\partial(R^2 j_{D_{ADP}})}{\partial x} - R^2 r_1 + 2Rr_4 \quad (7)$$

$$\frac{\partial(R^2 D_{ATP})}{\partial t} + \frac{\partial(R^2 D_{ATP}\dot{x})}{\partial x} = -\frac{\partial(R^2 j_{D_{ATP}})}{\partial x} + R^2 r_1 - 2Rr_3 \quad (8)$$

$$\frac{\partial(R^2 E)}{\partial t} + \frac{\partial(R^2 E\dot{x})}{\partial x} = -\frac{\partial(R^2 j_E)}{\partial x} + 2Rr_4 - 2Rr_2 \quad (9)$$

$$\frac{\partial(RD^*_{ATP})}{\partial t} + \frac{\partial(RD^*_{ATP}\dot{x})}{\partial x} = Rr_3 - Rr_2 \quad (10)$$

$$\frac{\partial(RD^*_{ATP} : E)}{\partial t} + \frac{\partial(RD^*_{ATP} : E\dot{x})}{\partial x} = Rr_2 - Rr_4 \quad (11)$$

$$r_1 = k_1 D_{ADP} \quad (12)$$

$$r_2 = k_2 D^*_{ATP} E \quad (13)$$

$$r_3 = (k_{3_1} + k_{3_2}(D^*_{ATP} + D^*_{ATP} : E))D_{ATP} \quad (14)$$

$$r_4 = k_4 D_{ATP} \quad (15)$$

In contrast to experimental and theoretical studies in literature, which assume a fixed space domain, the balance equations (7)-(11) describe the Min concentration waves on a membrane with varying length. As discussed above for the surfactant forming enzyme I, the cell growth has a diluting effect on the Min proteins. It is found in simulations that this dilution destroys the Min patterns rather quickly. To preserve the patterns, a continuous synthesis or dosage of Min proteins is required. The numerical results in section 2.5 will show that the patterns survive the cell growth, if $MinD$ and $MinE$ are fed in a spatially constant way along the whole length of the tube. We assume that the feeding is governed by a simple proportional controller. How such a proportional controller could be implemented experimentally in an artificial cell, is an open question. The introduction of a controller replaces equations (7) and (9) by equations (16) and (17), respectively:

$$\frac{\partial(R^2 D_{ADP})}{\partial t} + \frac{\partial(R^2 D_{ADP}\dot{x})}{\partial x} = -\frac{\partial(R^2 j_{D_{ADP}})}{\partial x} - R^2 r_1 + 2Rr_4 + K_g(D'_{ADP} - \overline{D_{ADP}}) \quad (16)$$

$$\frac{\partial(R^2 E)}{\partial t} + \frac{\partial(R^2 E\dot{x})}{\partial x} = -\frac{\partial(R^2 j_E)}{\partial x} + 2Rr_4 - 2Rr_2 + K_g(E' - \overline{E}), \quad (17)$$

with the controller gain K_g, the desired concentrations of $MinD_{ADP}$ and $MinE$ (denoted by D'_{ADP} and E') and the corresponding average concentrations of $MinD_{ADP}$ and $MinE$ (denoted by $\overline{D_{ADP}}$ and $\overline{E}$):

$$\overline{D_{ADP}} = \frac{\int(\pi R^2(D_{ADP} + D_{ATP}))\,\mathrm{d}x}{\int \pi R^2\,\mathrm{d}x} + \frac{\int(2\pi R(D^*_{ATP} + D^*_{ATP}E))\,\mathrm{d}x}{\int \pi R^2\,\mathrm{d}x} \quad (18)$$

$$\overline{E} = \frac{\int(\pi R^2 E + 2\pi R D^*_{ATP}E)\,\mathrm{d}x}{\int \pi R^2\,\mathrm{d}x} \quad (19)$$

2.3 Divisome

The third functional module that we consider is the divisome, whose task is to cut the cell into two halves by adding a contractile ring to the middle of the tube shaped membrane. There are different options for such a contractile ring. One possibility is the actin myosin system, which is involved in many motility, deformation and signal transduction processes of the cell (Zaidel-Bar et al., 2015). Myosin is a motor protein, which converts the chemical energy from the energy rich ATP molecule to mechanical energy (Cooper, 2000). Myosin attaches to actin fibers, crawls along the fibers and contracts them. An alternative approach for an artificial divisome might be the $FtsZ$ protein, which is known to play a role in cell division and is described as being able to contract by some authors (Li et al., 2007; Surovtsev et al., 2009).

In our mathematical model of the divisome module, we assume that there is some species Z that has the ability to contract and that preferably attaches to the membrane at places where the concentration of Min proteins is low. The model equations are derived from models for the actin myosin system by Lewis et al. (2014); George et al. (2013). We denote the concentration of the contractile protein in the cytosol as Z, and the membrane bound contractile protein as Z^*. Mass balances for both species result in equations (20) and (21):

$$\frac{\partial(R^2 Z)}{\partial t} + \frac{\partial(R^2 Z\dot{x})}{\partial x} = -\frac{\partial(R^2 j_Z)}{\partial x} - 2Rr_5 \quad (20)$$

$$\frac{\partial(R^2 Z^*)}{\partial t} + \frac{\partial(R^2 Z^*\dot{x})}{\partial x} = -\frac{\partial(RvZ^*)}{\partial x} + Rr_5 \quad (21)$$

The velocity v in the equation (21) denotes the movement of Z^* molecules on the membrane in x direction. The preference of Z to bind to membrane sites that are not occupied by Min molecules is captured by a simple adsorption rate expression r_5:

$$r_5 = k_5 Z(M_{max} - D^*_{ATP} - D^*_{ATP} : E) - k_5 k_{eqZ} Z^* \quad (22)$$

We assume that the membrane has a certain number of binding sites M_{max} which can be taken either by Min proteins or by Z^* molecules. The sites not occupied by Min proteins are free for the attachment of the contractile ring Z. k_5 is the rate constant of adsorption of the Z ring at the membrane and k_{eqZ} is a constant that describes the equilibrium state of Z ring attachment.

After the attachment to the membrane the Z ring causes the constriction of the cell. The Z ring formed from actin fibers is regarded as a viscoelastic and contractile gel (George et al., 2013; Lewis et al., 2014) and is calculated by the momentum balance:

$$\frac{\partial \rho v}{\partial t} = -\frac{\partial \rho v^2}{\partial x} - \frac{\partial(-\eta \frac{\partial v}{\partial x} - \sigma_C + \sigma_e)}{\partial x}, \quad (23)$$

where ρ represents the density of the Z ring fibers, v the velocity of the Z ring relative to the membrane and η the shear viscosity of the Z ring fibers. The contractile stress tensor σ_C is calculated as follows:

$$\sigma_C = \psi {Z^*}^2 exp(-\frac{Z^*}{Z_{sat}}), \quad (24)$$

where ψ is the constant for contractile stress and Z_{sat} is the saturation concentration of the Z ring. The elastic stress tensor σ_e is calculated by equation (25) using the elastic modulus constant g:

$$\sigma_e = gZ^*(e-1)) \quad (25)$$

The volumetric strain e is calculated by the following elasticity equation:

$$\frac{\partial Re}{\partial t} + \frac{\partial Re\dot{x}}{\partial x} = -\frac{\partial Rve}{\partial x} - R\lambda(e-1), \quad (26)$$

where λ is the relaxation rate of the Z fibers. The contractile stress tensor σ_C causes a radial contraction of the cell membrane. In principle, the resulting change of shape could be computed from a minimum bending energy model (Seifert et al., 1991; Surovtsev et al., 2009). In this work, we take a much simpler approach. We assume that the tubular membrane possesses a certain stiffness and does not change its radius, as long as σ_C is below a certain threshold σ_{buckle}. If σ_C exceeds this threshold, the membrane buckles, and its radius decreases quickly. The change of the radius during the constriction of the cell is defined by following equation:

$$\frac{\partial R}{\partial t} + \frac{\partial R\dot{x}}{\partial x} = -\frac{\partial R}{\partial x} + \frac{1}{T_{buckle}}(r_{ref} - R) \quad (27)$$

T_{buckle} is the time constant of buckling and the rate constant r_{ref} is calculated depending on the value of the contractile stress tensor σ_C:

$$r_{ref} = \begin{cases} R_0 & \text{for } \sigma_C < \sigma_{buckle} \\ R_{buckle} & \text{for } \sigma_C \geq \sigma_{buckle} \end{cases} \quad (28)$$

R_0 and R_{buckle} denote the membrane radius in relaxed state and after buckling, respectively.

2.4 Systemtheoretic representation of the coupled system

The modular nature of the cell model is illustrated by Fig. 3, showing the information flows between the three subsystems. The membrane module determines the shape of the cell and passes the geometrical information to the positioner module. Internally, the positioner module is represented by the Min concentration profiles and the corresponding spatial patterns, but the only output of the module is the desired position of the contractile ring. This output goes to the divisome module. The divisome module provides a contractile stress tensor as an output that couples back to the membrane module.

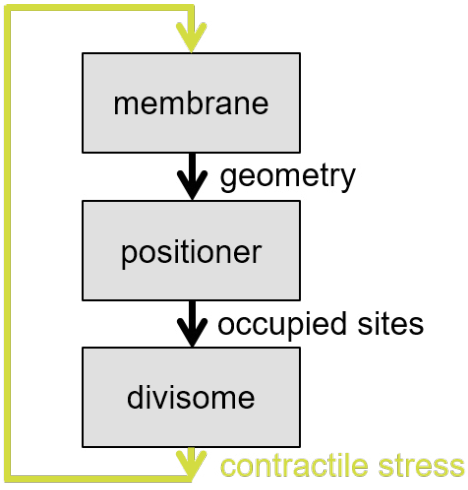

Fig. 3. Coupled system consisting of three modules: membrane, positioner and divisome.

On this abstract level, each of the three functional modules may be replaced by another subsystem providing the same functionality. For example, the Min patterns are not essential for the function of the positioner module, if one can find some other mechanism that places the divisome in the middle of the cell. There is an analogy to the design of chemical plants, where one finds the need for a process unit "separation", but may decide later, if this process unit is implemented as a distillation column, a chromatographic adsorption, a membrane device etc.

2.5 Simulation results

By coupling the shown subsystems we achieve a description of a growing cell like entity which is able to constrict in the middle of the cell and finally to divide.

Fig. 4 shows the coupled system of positioner and membrane. One can see that the tube becomes longer in the course of time. The plots show moving waves of the Min proteins on the membrane (multiple color bars), where high levels of the $MinD_{ATP} : MinE$ complex attached to the membrane are represented by red color and the low levels are blue. The central part of each plot represents the cytosol with the relative concentration of $MinE$ protein (red line) and the relative concentration of $MinD_{ADP}$

(blue line). It is obvious that the oscillations of the Min proteins stop after a certain time due to the dilution of the Min proteins.

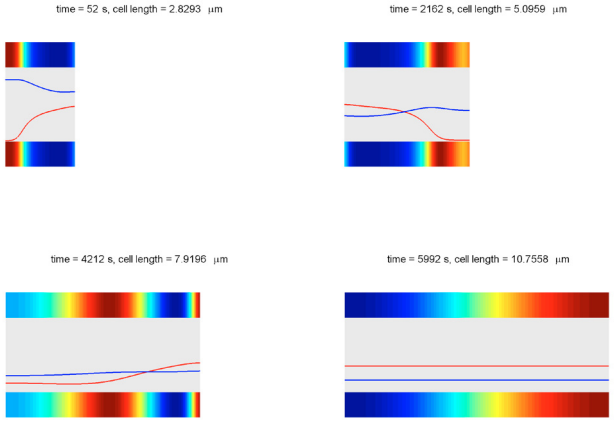

Fig. 4. Simulation results of coupled system of membrane and positioner. The upper and lower multiple color bars of each plot show the membrane bound Min proteins. High levels of Min proteins are represented by dark red color and low levels by dark blue. In the central area of each plot the cytosolic components concentrations are shown, $MinE$ protein by red line and $MinD_{ADP}$ protein by blue line.

To avoid the dilution of the Min proteins we implemented a coupled system of controlled positioner described by equations (16)-(19) and the membrane (Fig. 5). Here the controlled supply of Min proteins occurs, so the oscillations can be maintained.

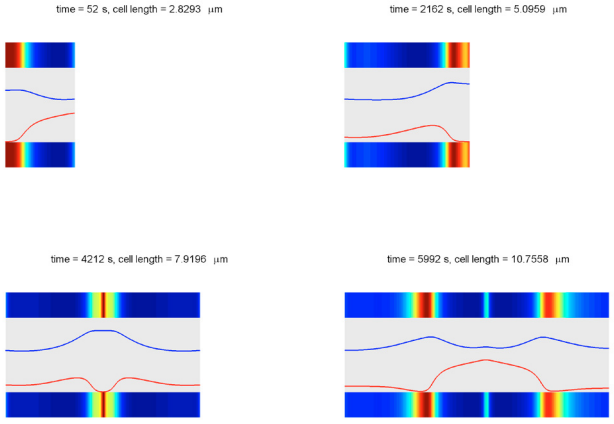

Fig. 5. Simulation results of coupled system of membrane and controlled positioner. The membrane bound Min proteins are shown by the upper and lower multiple color bars in each plot. The dark red color represents high concentrations of Min proteins and dark blue color represents low concentrations of Min proteins. The central area of each plot demonstrates the cytosolic components concentrations, red line is the $MinE$ protein and blue line $MinD_{ADP}$ protein.

Additionally we coupled the membrane, positioner and the divisome. Fig. 6 shows the simulation results. One can see the moving waves of the Min proteins on the membrane. At the middle area of the tube there is a low level of the $MinD_{ATP} : MinE$ complex, so Z ring formation is possible. Z ring accumulates on the membrane, which is represented by green increasing peaks. The cytosol is represented in the central area of each plot as before with relative concentration of $MinE$ protein (red line), relative concentration of $MinD_{ADP}$ (blue line) and the concentration of the cytosolic Z (green line).

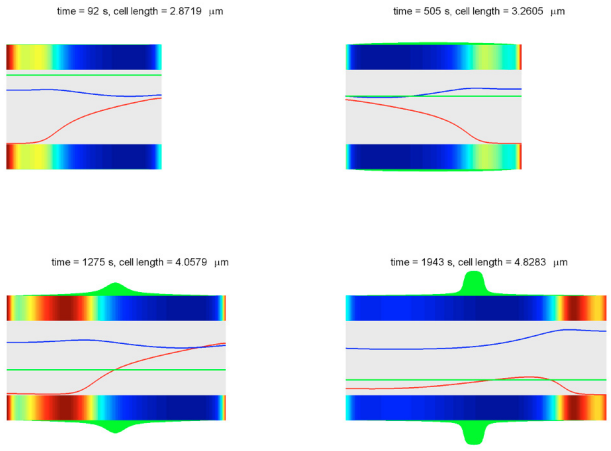

Fig. 6. Simulation results of coupled system of membrane, positioner and Z ring. The multiple color bars represent the membrane bound Min proteins. High concentrations of Min proteins are dark red colored and low concentrations dark blue. The cytosolic components concentrations are shown in the interspace of the multiple color bars, $MinE$ protein by red line, $MinD_{ADP}$ protein by blue line and the cytosolic Z by green line. The membrane bound Z^* is represented by the green peaks.

Fig. 7 shows the results of the implementation of radial constriction. It becomes apparent here that the membrane is able to constrict at any location. Thus the next step will be the controlled constriction in the middle of the tube with any necessary conditions for the progress of the constriction until cell division.

The implementation of the described model was done in ProMoT/DIANA (Ginkel et al., 2003; Mangold et al., 2014).

3. CONCLUSION

A model of a prospective artificial cell has been constructed from parts described by experimentally validated submodels. It turns out that throwing just together components for containment, vesicle growth, and division is not sufficient to obtain a reproducing cell. Instead, the approach reveals deficiencies of the assembled system that may be remedied by adding appropriate regulating instances. The simulation results of the artificial cell allow the formulation of control tasks to specify these regulators. In the considered example, the identified control tasks

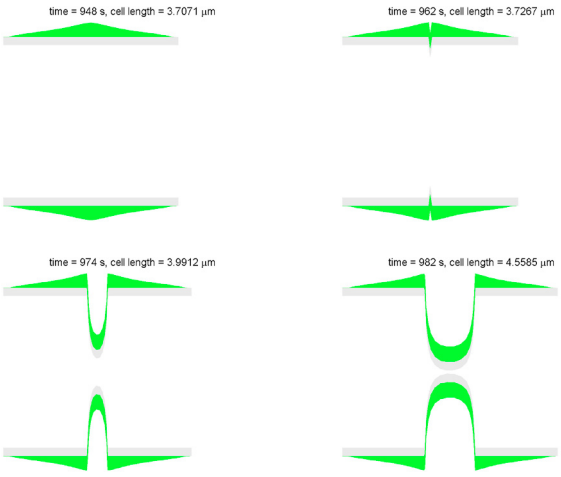

Fig. 7. Simulation results of coupled system of membrane and Z ring. The membrane bound contractile protein Z^* is represented by the green peaks that invaginates and constricts the membrane.

are (i) to prevent the depletion of enzyme I, (ii) to keep the Min concentrations on a certain level, and (iii) to synchronize the growth of the tube shaped membrane and the growth of the contractile ring. Currently, the simulated assembled system does not contain solutions for these tasks that can be implemented in experiments, but it may give some indications how these solutions should look like; e.g. it is found that a spatially constant dosing of Min proteins suffices to preserve the pattern formation, more sophisticated feeding strategies are not required. A weak point of the presented model is that energy consumption and energy supply are completely ignored at the moment. Adding an energy module should be the next step towards a more realistic model of an artificial cell.

ACKNOWLEDGEMENTS

This work is part of the MaxSynBio consortium which is jointly funded by the Federal Ministry of Education and Research of Germany and the Max Planck Society.

REFERENCES

Cooper, G.M. (2000). Actin, Myosin, and Cell Movement. URL `http://www.ncbi.nlm.nih.gov/books/NBK9961/`.

George, U.Z., Stphanou, A., and Madzvamuse, A. (2013). Mathematical modelling and numerical simulations of actin dynamics in the eukaryotic cell. *Journal of Mathematical Biology*, 66(3), 547–593.

Ginkel, M., Kremling, A., Nutsch, T., Rehner, R., and Gilles, E.D. (2003). Modular modeling of cellular systems with ProMoT/diva. *Bioinformatics*, 19(9), 1169–1176. doi:10.1093/bioinformatics/btg128.

Huang, K.C., Meir, Y., and Wingreen, N.S. (2003). Dynamic structures in Escherichia coli: Spontaneous formation of MinE rings and MinD polar zones. *Proceedings of the National Academy of Sciences*, 100(22), 12724–12728.

Karr, J.R., Sanghvi, J.C., Macklin, D.N., Gutschow, M.V., Jacobs, J.M., Bolival, B., Assad-Garcia, N., Glass, J.I., and Covert, M.W. (2012). A Whole-Cell Computational Model Predicts Phenotype from Genotype. *Cell*, 150(2), 389–401. doi:10.1016/j.cell.2012.05.044.

Keasling, J.D. (2008). Synthetic Biology for Synthetic Chemistry. *ACS Chemical Biology*, 3(1), 64–76. doi:10.1021/cb7002434.

Keasling, J.D. (2012). Synthetic biology and the development of tools for metabolic engineering. *Metabolic Engineering*, 14(3), 189–195. doi:10.1016/j.ymben.2012.01.004.

Lewis, O.L., Guy, R.D., and Allard, J.F. (2014). Actin-myosin spatial patterns from a simplified isotropic viscoelastic model. *Biophysical Journal*, 107(4), 863–870.

Li, Z., Trimble, M.J., Brun, Y.V., and Jensen, G.J. (2007). The structure of FtsZ filaments in vivo suggests a force-generating role in cell division. *The EMBO journal*, 26(22), 4694–4708. doi:10.1038/sj.emboj.7601895.

Loose, M., Fischer-Friedrich, E., Ries, J., Kruse, K., and Schwille, P. (2008). Spatial regulators for bacterial cell division self-organize into surface waves in vitro. *Science*, 320(5877), 789–792.

Mangold, M., Khlopov, D., Danker, G., Palis, S., Svjatnyj, V., and Kienle, A. (2014). Development and nonlinear analysis of dynamic plant models in ProMoT /diana. *Chemie Ingenieur Technik*, 86(7), 1107–1116. doi:10.1002/cite.201400003.

Mavelli, F., Altamura, E., Cassidei, L., and Stano, P. (2014). Recent theoretical approaches to minimal artificial cells. *Entropy*, 16(5), 2488–2511.

Rollié, S., Mangold, M., and Sundmacher, K. (2012). Designing biological systems: Systems Engineering meets Synthetic Biology. *Chemical Engineering Science*, 69(1), 1–29. doi:10.1016/j.ces.2011.10.068.

Schweizer, J., Loose, M., Bonny, M., Kruse, K., Monch, I., and Schwille, P. (2012). Geometry sensing by self-organized protein patterns. *Proceedings of the National Academy of Sciences of the United States of America*, 109(38), 15283–15288.

Schwille, P. (2011). Bottom-Up Synthetic Biology: Engineering in a Tinkerers World. *Science*, 333(6047), 1252–1254. doi:10.1126/science.1211701.

Seifert, U., Berndl, K., and Lipowsky, R. (1991). Shape transformations of vesicles: Phase diagram for spontaneous-curvature and bilayer-coupling models. *Physical Review A*, 44(2), 1182–1202.

Surovtsev, I.V., Zhang, Z., Lindahl, P.A., and Morgan, J.J. (2009). Mathematical modeling of a minimal protocell with coordinated growth and division. *Journal of Theoretical Biology*, 260(3), 422–429. doi:10.1016/j.jtbi.2009.06.001.

Trosset, J.Y. and Carbonell, P. (2015). Synthetic biology for pharmaceutical drug discovery. *Drug Design, Development and Therapy*, 9, 6285–6302. doi:10.2147/DDDT.S58049.

Zaidel-Bar, R., Zhenhuan, G., and Luxenburg, C. (2015). The contractome a systems view of actomyosin contractility in non-muscle cells. *J Cell Sci*, 128(12), 2209–2217. doi:10.1242/jcs.170068.